Microporous and Mesoporous Materials 245 (2017) 64–72

Contents lists available at ScienceDirect

Microporous and Mesoporous Materials

journal homepage: www.elsevier.com/locate/micromeso

Kaolin-based magnetic zeolites A and P as water softeners

Raquel de Andrade Bessa [a], Luelc de Sousa Costa [b], Cristiane Pinto Oliveira [a], Felipe Bohn [c], Ronaldo Ferreira do Nascimento [d], José Marcos Sasaki [e], Adonay Rodrigues Loiola [a, *]

[a] Departamento de Química Orgânica e Inorgânica, Universidade Federal do Ceará, Campus do Pici, 60440-900 Fortaleza, CE, Brazil
[b] Departamento de Química Inorgânica, Instituto de Química, Universidade Estadual de Campinas, Cidade Universitária II, 13083-000 Campinas, SP, Brazil
[c] Departamento de Física, Universidade Federal do Rio Grande do Norte, 59078-900 Natal, RN, Brazil
[d] Departamento de Química Analítica e Físico-Química, Universidade Federal do Ceará, Campus do Pici, 60440-900 Fortaleza, CE, Brazil
[e] Departamento de Física, Universidade Federal do Ceará, Campus do Pici, 60440-900 Fortaleza, CE, Brazil

ARTICLE INFO

Article history:
Received 20 February 2017
Received in revised form
4 March 2017
Accepted 5 March 2017
Available online 7 March 2017

Keywords:
Zeolite A
Zeolite P
Magnetic zeolites
Magnetite nanoparticles

ABSTRACT

In this work, we report an experimental investigation on the synthesis of zeolites A and P, using kaolin as the main SiO_2 and Al_2O_3 sources, by hydrothermal route, as well as on the structural, spectroscopic and magnetic properties of the produced zeolite composites with magnetite nanoparticles. The zeolites were successfully synthesized and the characterization of the obtained materials was carried out considering different techniques, including X-ray diffraction (XRD), infrared vibrational spectroscopy, scanning electron microscopy (SEM), transmission electron microscopy (TEM), as well as measurements of the magnetization as a function of the temperature and applied magnetic field. XRD analysis confirmed zeolites A and P as main crystalline phases, with a low intensity peak regarding the presence of small quantities of quartz remaining from the unreacted clay. SEM showed the well-defined morphologies of zeolites and, in the composites, magnetite nanoparticles dispersed over their surface. The average size of the magnetite nanoparticles was *ca.* 50 nm as determined by TEM analyses. The magnetic characterization confirmed the ferrimagnetic behavior of the magnetite nanoparticles and of the composites, as well as verified that the magnetic properties of the nanoparticles are not affected by the zeolites in the composite formation. Thus, the results evidenced that high quality zeolite composites with magnetite nanoparticles can be reached by considering the employed low cost method, placing this route as an attractive alternative for water softening reaching removal levels of about 97% in the first application times.

1. Introduction

Zeolites materials are of immense fundamental and industry importance, being widely used, for instance, as commercial adsorbents and catalysts. For this reason, these systems have attracted increasing interest, a fact evidenced by the growing number of reports devoted to this issue [1–4].

Zeolites are defined as porous aluminosilicates with crystalline structure formed by the combination of tetrahedral $[SiO_4]^{4-}$ and $[AlO_4]^{5-}$ joined by oxygen atoms [5]. In particular, the chemical composition of the zeolites is often and conveniently represented by:

$$A^{m+}_{y/m}[(SiO_2)_x \cdot (AlO_2^-)_y] \cdot zH_2O,$$

where A is a cation with charge m, $(x + y)$ is the number of tetrahedra per crystallographic unit cell, and x:y is the silicon:aluminum ratio. Based on the celebrated Löwenstein's rule, Al–O–Al linkages are not allowed and $y/x \geq 1$ [6].

There are numerous zeolite synthesis methods reported [7–13]. Among them, the hydrothermal method appears as the most important. The hydrothermal term is used in a wide sense and also includes zeolite crystallization from aqueous systems containing the necessary chemical components [14]. The selectivity of synthesis represents one of the toughest difficulties in the obtainment of zeolites in the laboratory. Zeolites are metastable phases, *i.e.*, other zeolite types may be formed if the synthesis processes go on, and just a few changes in the synthesis conditions may give rise to impure phases through co-crystallization of other phases apart from the one desired. Although they have similar constituents, their

* Corresponding author.
E-mail address: adonay@ufc.br (A.R. Loiola).

http://dx.doi.org/10.1016/j.micromeso.2017.03.004
1387-1811/

properties may be different (*e.g.* zeolite A and zeolite X). As result of the synthesis process complexity, many zeolites are obtained by empirical methods carried out by heating procedures using structure-directing agents (SDA) [11], in conditions that lead to the synthesis of the desired phase. However, these procedures performed in the laboratory would hardly adapt themselves to the industrial scale [15]. For this reason, the sol-gel formation has become one of the main synthesis methods [8], together with the use of surfactants as SDA [16]. Additionally, the use of other synthesis techniques involving ultrasound and microwaves has also been considered and reported through some works found in literature [17–19].

In order to reduce the costs of the production, alternative sources for zeolite synthesis have been employed [20]. Thus, due to its SiO_2 and Al_2O_3 content, kaolin has been widely used for this purpose [21–27]. Kaolin is a clay in which the major constituent is the clay mineral kaolinite, $Al_2Si_2O_5(OH)_4$, a dioctahedrical layered hydrated aluminosilicate of the 1:1 type with two distinct interlayer surfaces. Hence, since kaolinite-based zeolites are produced from cheaper natural materials, where pure sodium silicate and sodium aluminate are considered, they appears as an attractive alternative system especially regarding the cost efficiency [28].

Zeolites have attracted attention of the chemical industry due to their many interesting properties. For instance, zeolite high cation exchange capacity allows its use to remove heavy metal cations from industrial effluents. However, one of the main challenges related to the zeolite reuse after removing cations in solution resides in its separation, which in general requires expensive techniques. To overcome it, one promising alternative is the zeolite composites with magnetic properties [29,30]. For this purpose, an interesting route corresponds to the possibility of dispersion of magnetic nanoparticles over the zeolite surface, forming the zeolite composite.

Magnetic nanoparticles have unique physicochemical, magnetic, and optical properties that are of great importance in diverse applications. Cobalt, iron, and iron oxides nanoparticles, such as maghemite and magnetite, have been widely considered as the most suitable materials for production of magnetic nanocomposites due to their significant magnetic properties [31]. Several methods for synthesizing iron oxide/zeolite have been proposed and investigated [32,33]. However, a thorough comprehension of them is still limited and, for this reason, further investigations on this issue are still required.

In this work, we report an experimental investigation on the synthesis of zeolites A and P, using kaolin as the main SiO_2 and Al_2O_3 sources, by hydrothermal route, as well as on the structural, spectroscopic and magnetic properties of the produced zeolite composites with magnetite nanoparticles. In particular, by considering a wide range of techniques, we explore the possibility of obtainment of high quality zeolite composites with magnetite nanoparticles by a low cost method. We also performed essays to assess the efficiency of these materials as water softeners.

2. Experimental

2.1. Synthesis

For this study, we produced zeolites A and P composites with magnetite nanoparticles. To this end, kaolin supplied by Rocha Minérios (PB-Brazil) was previously treated at 600 °C for 2 h in order to induce its conversion to metakaolin, a more reactive product. Zeolite A was synthesized by hydrothermal route with a gel produced by mixing 1.00 g of metakaolin with 12 mL of NaOH 2.8 mol L^{-1}. This precursor gel was transferred to a Teflon-lined stainless steel autoclave and crystallized by thermal treatment under autogenous pressure and static conditions at 100 °C for 4 h. The obtained solid was washed several times with distilled water until constant pH and dried at 80 °C overnight [34]. Zeolite P was synthesized following similar procedures, but with the precursor gel prepared by mixing 1.09 g of metakaolin with 2.07 g of Na_2SiO_3 and 20 mL of NaOH 0.98 mol L^{-1}. The crystallization took place at 100 °C for 48 h [25]. The obtained material was also washed and dried, as described for zeolite A. The magnetic nanoparticles were synthesized by Fe^{2+} precipitation/partial oxidation. In this case, 5 mL of NaOH 2.5 mol L^{-1} solution was added slowly by means of 250 μL aliquots at intervals of 30 s into 100 mL of $FeSO_47H_2O$ 0.065 mol L^{-1}, under mechanical stirring at 50 °C [35]. The solid nanoparticles were separated using a magnet. The nanoparticles were washed with distilled water and acetone. The composites were prepared by mixing the zeolites and the magnetic nanoparticles in a 3:1 mass ratio, macerated and dispersed in distilled water at 80 °C for 1 h.

2.2. Characterization

We have characterized the structural, spectroscopic and magnetic properties of the produced zeolites A and P composites with magnetite nanoparticles. In this case, we considered different techniques, including X-ray diffraction (XRD), infrared vibrational spectroscopy (FTIR), scanning electron microscopy (SEM), transmission electron microscopy (TEM), as well as measurements of the magnetization as a function of the temperature and applied magnetic field.

2.2.1. X-ray diffraction

XRD experiments were performed using a Panalytical (X-Pert Pro MPD) x-ray powder diffractometer. The powder patterns were collected in the continuous mode with 2θ scan speed of 0.5° min^{-1}. Co-Kα radiation was used, obtained with the tube operating at 40 kV and 40 mA. For the diffraction measurements, we selected samples with particle sizes below 75 μm (200 mesh).

2.2.2. Infrared vibrational spectroscopy

Fourier transform infrared (FTIR) spectra were obtained by using a Shimadzu IRealise FTIR spectrometer in the 4000-400 cm^{-1} region, with nominal resolution of 2 cm^{-1}. For these experiments, the samples were prepared in KBr wafers.

2.2.3. Scanning electron microscopy (SEM)

SEM analyses were carried out in a FEG equipment model Quanta 450. The non-magnetic samples were prepared on double-sided carbon tape on an aluminum support and coated with a thin layer of gold. For the magnetic samples, colloidal silver paste was used instead of double-sided carbon tape.

2.2.4. Transmission electron microscopy (TEM)

TEM analyses of the magnetic nanoparticles were performed by using a few milligrams of the sample, in the powder form, dispersed in isopropyl alcohol and sonicated for 15 min. Two drops of the dispersion were placed onto ultra-thin carbon coated copper grids. After deposition, the samples were dried at room temperature overnight prior to the obtainment of the images. The images were acquired using a JEOL JEM 2100 LaB_6 operating at an accelerating voltage equal to 200 kV and equipped with a TV (Gatan ES500 W).

2.2.5. Magnetic properties

Magnetic measurements were carried out using a vibrating sample magnetometer module in a Physical Property Measurement System (PPMS), Quantum Design. In this case, magnetization

curves, with magnetic fields up to 15 kG, were acquired at the specific temperatures of 5 K and 300 K. Moreover, zero field cooling (ZFC) and field cooling (FC) magnetization measurements were performed in the range of temperature between 5 K and 300 K, with a probe field of 70 G.

2.3. Water softening

Softening processes were carried out in order to evaluated zeolites A, P, and zeolites A and P magnetic composites capacity as cation exchangers in solution, removing Ca^{2+} and delivering Na^{+}. Samples of 20 mL of a 110 mg L^{-1} Ca^{2+} solution were transferred to 125 mL erlenmeyers. The mass of the softening used were: 30 mg of either zeolite A or zeolite P and 40 mg of either zeolite A magnetic composite or zeolite P magnetic composite (as the zeolite nanoparticle mass ratio is 3:1, it is equivalent to 30 mg of the zeolite) to each erlenmeyer. The samples were stirred for 1–120 min, in triplicate, filtered and analyzed by flame photometry. In order to determine the maximum capacity of ion exchange of zeolites and zeolites composites, samples of 20 mL of a 110 mg L^{-1} Ca^{2+} solution were treated, in similar conditions, but using zeolites mass of 3–90 mg and zeolite composites mass of 4–120 mg (the same mass of zeolite).

3. Results and discussion

Here, we present the wide characterization of the studied zeolites A and P composites with magnetite nanoparticles, and confirm the quality of the samples produced from kaolin by hydrothermal route.

3.1. XRD

Fig. 1 presents the XRD powder patterns of kaolin (1a) and metakaolin (1b). The chemical composition of kaolin is dependent on its origin region. Thus, from its pattern, it is verified that, although kaolinite (ICSD 68698) [36] is the major constituent, other minor phases, as well as quartz (ICSD 67117) [37] and halloysite (AMCSD 18094) [38], may be found. Metakaolin results from the thermal decomposition of kaolin, as attested by the low crystallinity showed in its XRD pattern. This way, it becomes suitable to the zeolite synthesis, once its reactivity in alkali solution increases.

Fig. 2 shows the XRD patterns of the composites produced from each zeolite and the nanoparticles, as well as of the zeolites A and P

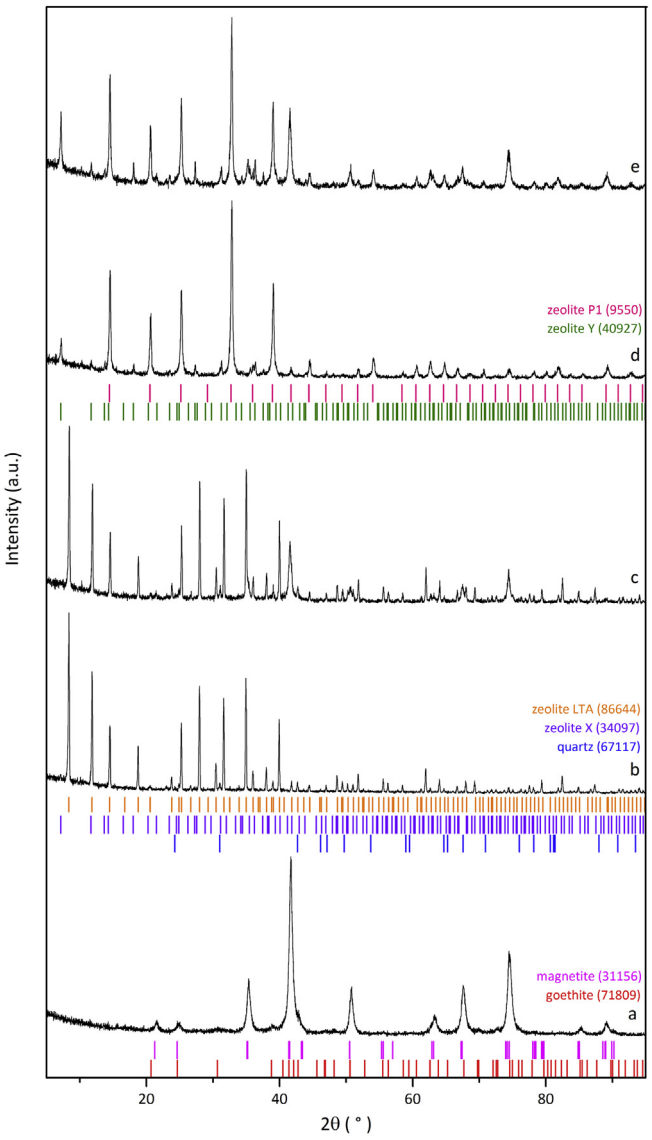

Fig. 2. XRD patterns of (a) magnetic nanoparticles, (b) zeolite A, (c) zeolite A magnetic composite, (d) zeolite P and (e) zeolite P magnetic composite.

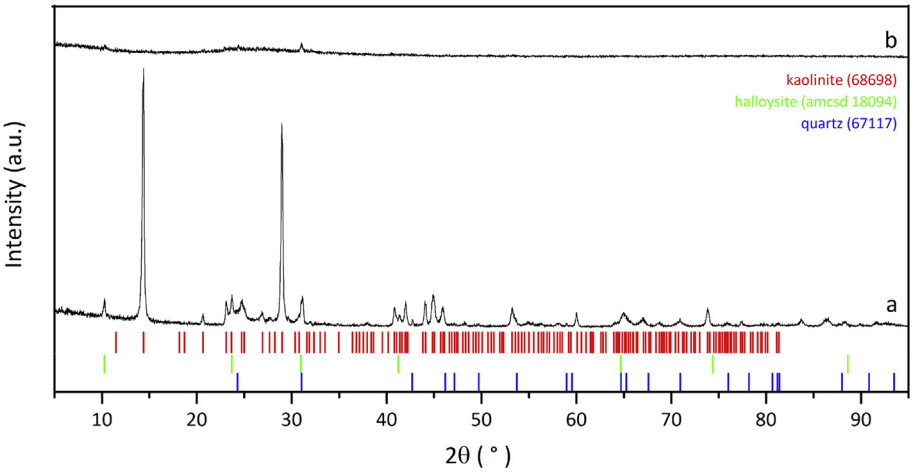

Fig. 1. XRD patterns of (a) kaolin and (b) metakaolin.

and the magnetic nanoparticles. The powder patterns obtained for the zeolites A and P show well-defined peaks referent to the expected phases of zeolite A (ICSD 86644) [39] and zeolite P (ICSD 9550) [40] as well as small amounts of secondary phases of quartz (ICSD 67117) [37] in both samples, a fact assigned by a low intensity peak at 31° (2θ) possibly remaining from the kaolin used in the syntheses (as attested in Fig. 1(b)), and zeolite X (ICSD 34097) [41] in zeolite A sample and zeolite Y (ICSD 40927) [42] in zeolite P sample. In particular, the results evidences that the zeolites A and P are the main crystalline phases of the respective composites, as depicted from the intense and well defined peaks shared in the XRD pattern of all samples. The pattern of magnetic nanoparticle was consistent to magnetite - Fe_3O_4 (ICSD 31156) [43], and a low intensity peak related to the most intense peak of goethite - FeO(OH) (ICSD 71809) [44] was also identified. In XRD patterns of zeolite A (Fig. 2(c)) and zeolite P composite samples (Fig. 2(e)), it was possible to identify the main peak of magnetite phase, at 41.5° (2θ).

Table 1 presents the Rietveld refinement data obtained using the General Structure Analysis System (GSAS) software [45] through the EXPGUI interface [46]. It is possible to testify the main crystalline phases identified previously, as well as the weight composition in the samples and the crystallite size.

Table 1
Rietveld refinement output. The major phases are indicated in bold.

Sample	Phase	% Weight	χ^2
Kaolin	**Kaolinite**	**78.0**	1.591
	Halloysite	21.0	
	Quartz	1.0	
Magnetic nanoparticles	**Magnetite**	**91.6**	0.8524
	Goethite	8.4	
Zeolite A	**Zeolite A**	**98.8**	1.223
	Zeolite X	0.3	
	Quartz	0.9	
Zeolite A magnetic composite	**Zeolite A**	**85.9**	1.240
	Magnetite	12.9	
	Quartz	1.2	
Zeolite P	**Zeolite P**	**95.7**	1.031
	Zeolite Y	3.0	
	Quartz	1.3	
Zeolite P magnetic composite	**Zeolite P**	**70.7**	1.097
	Magnetite	15.1	
	Zeolite Y	11.4	
	Quartz	2.8	

The refinement quality is indicated through the χ^2 parameter provided in the end of each refinement cycle, indicating the adjustment between the observed and the calculated patterns. These values need to be close to 1.0 for χ^2, as it was found in all the samples analyzed in this work, which means a high degree of adjustment for the identified phases. The provided weight % shows the majority phases as indicated in the graphs in Figs. 1 and 2 in addition to the secondary phases that can be produced in the same compositional pattern (Na_2O–Al_2O_3–SiO_2–H_2O) as competing phases.

3.2. FTIR

Vibrational spectroscopy in the infrared provides additional information to the structural analysis performed by XRD. In this context, information on the basic structure of the zeolite is required in order to make the correct allocation of the absorption bands found.

Fig. 3 shows the spectra of kaolin (3a) and metakaolin (3b). Kaolin presents at least 20 well-defined FTIR bands in the region of 1400–400 cm^{-1} due to Si–O, Si–O–Al, and Al–OH vibrations [47]. The conversion to metakaolin completely removes these bands, leaving a broad intense asymmetric band at 1095 cm^{-1} as the main feature. Moreover, the disappearance of the bands at 914 and 937 cm^{-1} indicates the loss of Al–OH units [48]. In comparison to Fig. 4 (b and d), the appearance of bands associated with the zeolite structure indicates the transformation of kaolin to zeolites A and P.

The FTIR spectra of the composites produced from each zeolite and the nanoparticles, as well as of the zeolites A and P and the magnetic nanoparticles, are presented in Fig. 4. From the comparison among these spectra, it is possible to verify that the composites formation promoted just a slight decrease in the zeolites characteristic bands intensities, specially for zeolite A (Fig. 4(b-c)) and the magnetite bands were not identified in the spectra possibly because there is overlap of these bands with those identified for zeolites.

The magnetic nanoparticles do not show bands in the region around 1000 cm^{-1}, relating to the asymmetric stretch of the T–O

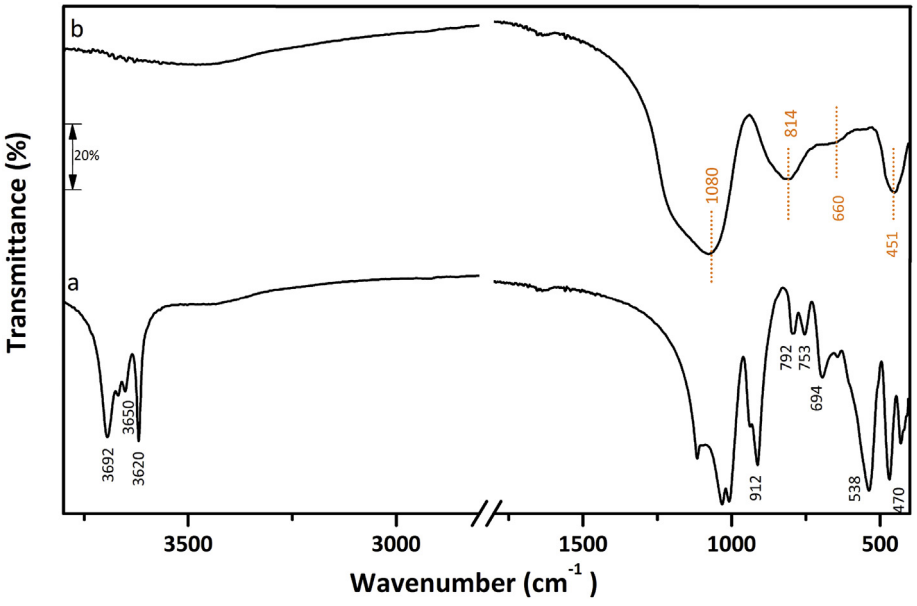

Fig. 3. FTIR spectra of (a) kaolin and (b) metakaolin.

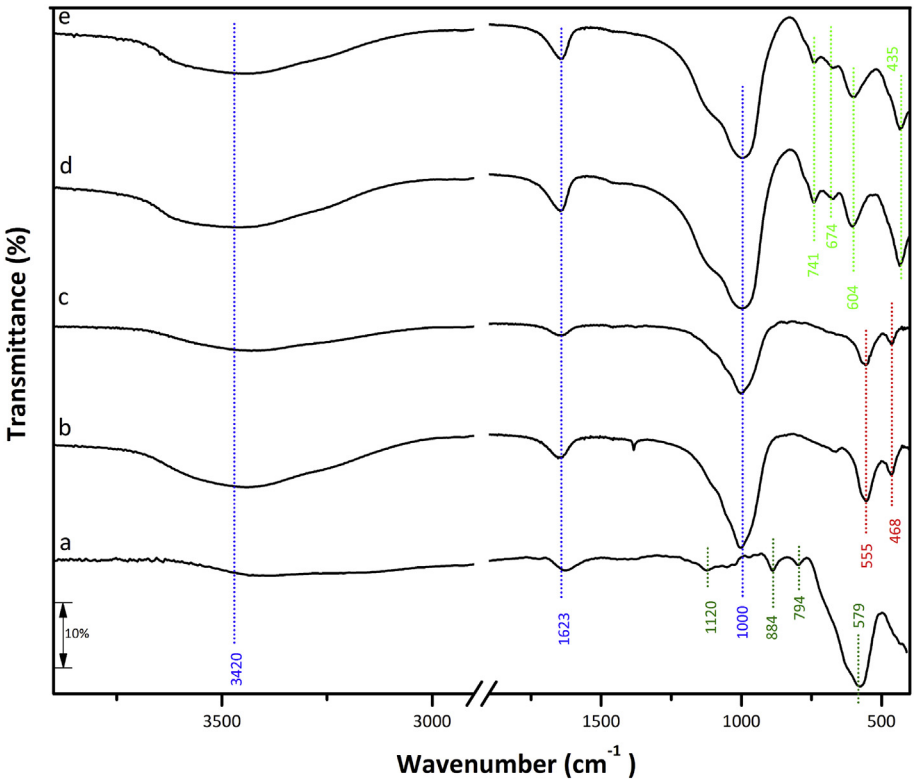

Fig. 4. FTIR spectra of (a) magnetic nanoparticles, (b) zeolite A, (c) zeolite A composite, (d) zeolite P and (e) zeolite P composite.

bonds of the zeolite structure [49], and the presence of free water (the 3420 cm^{-1} band) [50] and sulfate groups (at 1120 and 1623 cm^{-1}) [51] can be distinguished. These bands appear in small intensities and probably those identified groups emerged from the synthesis process during the washing step, which did not eliminate them completely, once the precursor material was iron sulfate.

Low-intensity bands are also identified for the magnetic nanoparticle sample, Fig. 4(e), and a well-defined band at 579 cm^{-1}, which can be attributed to the characteristic Fe—O vibration in magnetite [52]. The bands at 794 and 884 cm^{-1} are related to the Fe—O—H bending vibrations in the structure of the small portions of goethite [51]. Previous woks [51,53] reported the presence of bands characteristic of ferrite but in regions below 400 cm^{-1}, which could not be observed in the presented spectra.

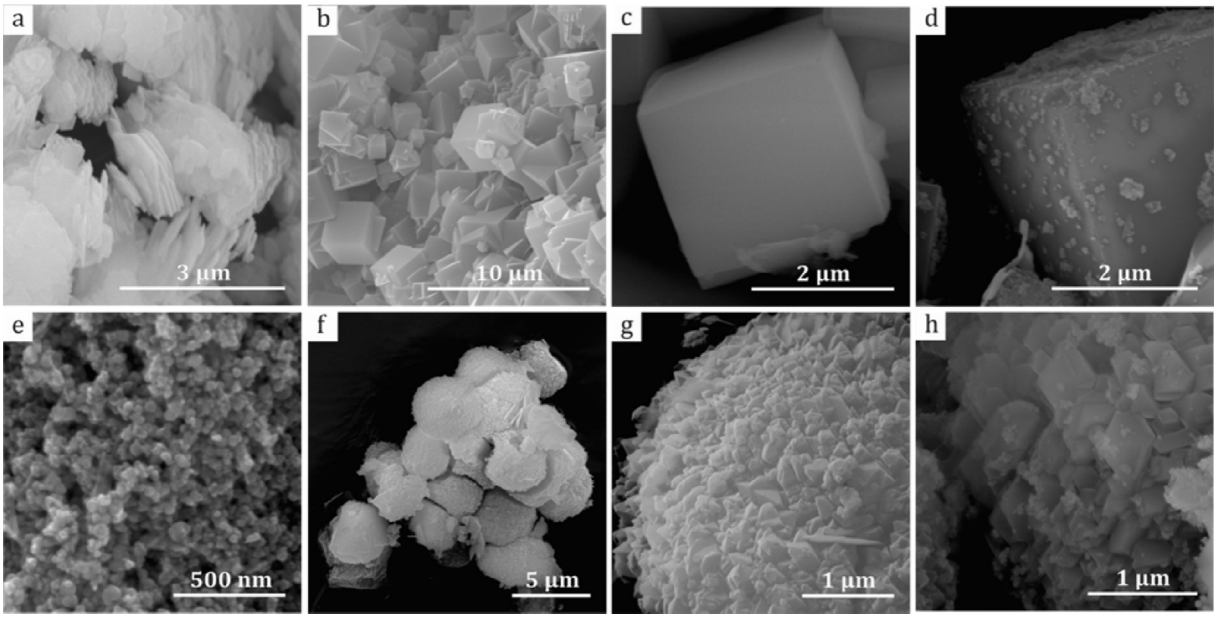

Fig. 5. SEM images of (a) kaolin, (b,c) zeolite A, (d) zeolite A composite, (e) magnetic nanoparticles, (f,g) zeolite P and (h) zeolite P composite.

3.3. SEM

SEM images of all the samples are presented in Fig. 5. From Fig. 5(a), it can be observed that kaolin consists predominantly of agglomerated particles with stacking booklet type and pseudo-hexagonal crystals characteristic of kaolinite, its major clay mineral constituent [25]. SEM analysis of the magnetic nanoparticles, Fig. 5(e), indicates particles with a tendency of spherical shape as well as a homogenous particle size distribution with sizes of *ca.* 50 nm. Fig. 5(b and c) shows the micrographs of zeolite A. The characteristic zeolite A cubic crystals with homogeneous size distribution (*ca.* 1 μm) are revealed. Fig. 5(f and g) shows the micrographs of zeolite P, which presents pseudo-spherical forms generated from needle-like crystals clusters with average sizes of *ca*. 5 μm [54]. Considering the SEM images of zeolites A and P, Fig. 5(b,c,f,g), it is not possible to identify unreacted kaolin, which is in accordance to that observed in the correspondent XRD patterns.

The micrographs of the composites, Fig. 5(d) and (h), evidence that the nanoparticles are dispersed over the zeolite surfaces, distributed thought all the samples. Zeolites composites are formed by means of a physical process of impregnation of the magnetic nanoparticles over the zeolites surfaces. To the formation of the composite, it is critical a considerable size difference between the zeolites and the nanoparticles. The micrographs of the composites, as seen in Fig. 5(d) for zeolite A composite and in Fig. 5(h) for zeolite P composite, allow the identification of the zeolites surfaces covered by the magnetic particles. In fact, a uniform distribution of magnetic nanoparticles over zeolite surfaces can be observed, which indicates some interaction between the materials. Therefore they can respond to a magnet allowing the zeolites to be attracted to it and this way being separated from other media as, for instance, aqueous solutions.

Photographs of the synthesized samples are shown in Fig. 6. Pure zeolites appear as white powders without attraction to the magnet. On the other hand, the magnetic nanoparticles are black powder, strongly attracted to approaching magnet. The composites are brown powders and have similar characteristics to the magnetic nanoparticles regarding the attraction to the magnet.

3.4. TEM

By means of the TEM images of the magnetic nanoparticles shown in Fig. 7, it is possible to visualize the spherical morphology, typical of magnetite [55,56], with sizes comprising between 20 and 100 nm. Such variation may be related to the crystals maturation process during their growing [57]. The agglomeration of nanoparticles, as indicated in the granulometric distribution histogram, presented in Supplementary Data, is observable in the darker regions of the micrographs. Although in very small quantities, it is also possible to visualize nanorods, which may be associated to presence of goethite [56,58,59], corroborating the FTIR data.

3.5. Magnetic properties

On the magnetic properties, Fig. 8 shows the magnetization curves and ZFC and FC curves of the zeolite A and P composites and

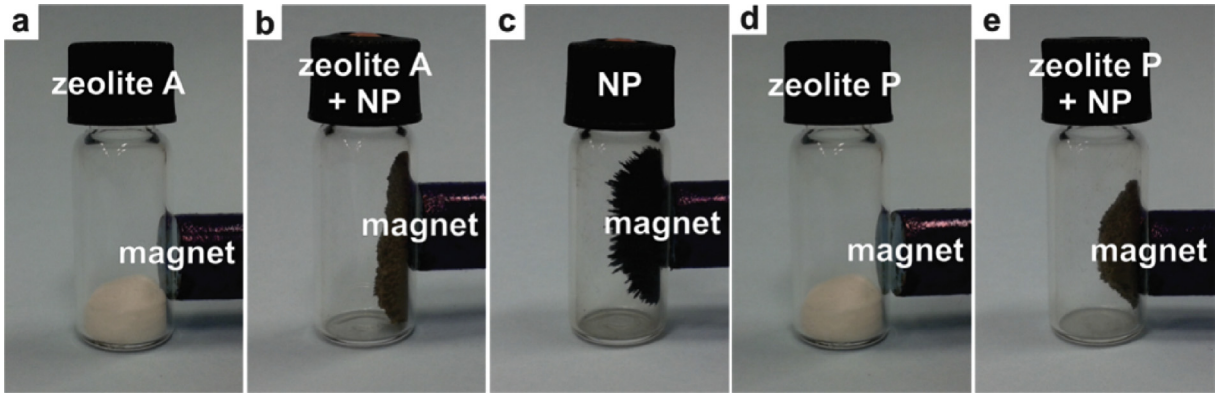

Fig. 6. Photograph presenting the response to the magnet of the (a) zeolite A, (b) zeolite A composite, (c) magnetic nanoparticles, (d) zeolite P, and (e) zeolite P composite.

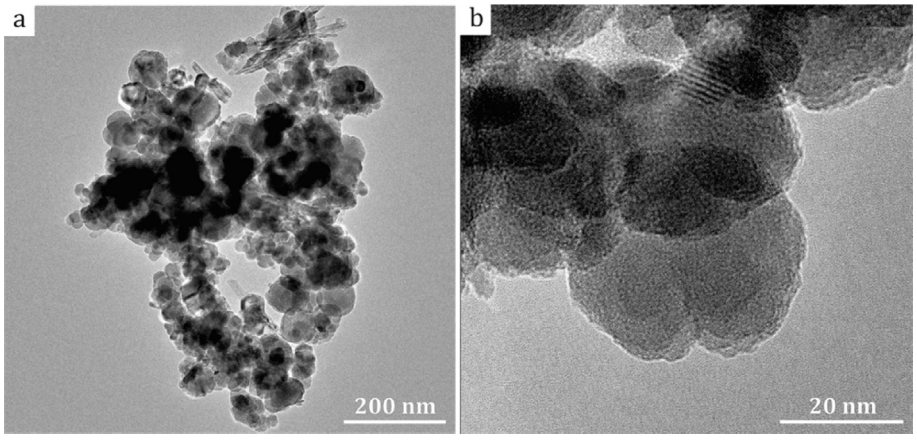

Fig. 7. TEM images of magnetic particles.

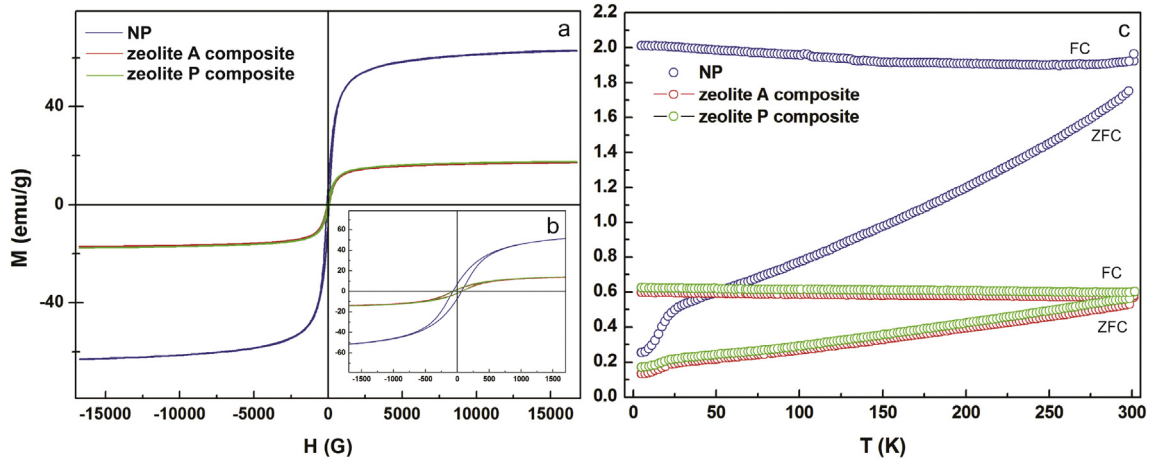

Fig. 8. (a) Magnetization curves (MxH) at 300 K, (b) zoom of the MxH at 300 K at low magnetic field values, and (c) FC and ZFC magnetization measurements of the magnetic nanoparticles (NP), zeolite A composite and zeolite P composite.

of the magnetite nanoparticles. From the MxH curve at 300 K in Fig. 8(a), at a first glance, a superparamagnetic-like behavior may be inferred. However, a closer inspection revealed hysteretic curves, as shown in Fig. 8(b), indicating a blocked state. Given the composition of the nanoparticles, it suggests a ferrimagnetic ordering for all samples at room temperature, a behavior in concordance with previous reports on magnetite nanoparticles found in literature [60–65]. The samples present the very same coercive field, having values of ~365 G at 5 K, not shown here, and ~70 G at 300 K. The remarkable similarity of the shape of the curves and coercive field values suggests that the nanoparticles keep their main features and do not present any modification in their magnetic properties when incorporated onto the zeolite surface. The magnetite nanoparticles have saturation magnetization of ~72 emu/g at 5 K, not shown, and ~63 emu/g at 300 K, both below the value observed for bulk magnetite, 92 emu/g [64]. This is expected since the magnetic properties in nanoparticles are strongly influenced by finite size effects and the breaking of the crystal symmetry at the particle surface [61]. On the other hand, the composites have ~25.5 emu/g and ~17.5 emu/g, at 5 K and 300 K, respectively. The reduction of the saturation magnetization, and consequently remanent magnetization, observed in the composites when compared to the magnetic nanoparticles is not surprising, being directly proportional to the increase of mass of the non-magnetic material, *i.e.*, to the mass of zeolite.

Regarding the ZFC and FC curves in Fig. 8(c), they are diverse from that expected for a superparamagnetic-like behavior, and present typical features of an ordered magnetic system, whereas a relatively weak magnetic field is enough to split the curves. The shape of the curves confirms that the magnetic properties of the magnetic nanoparticles are not affect by the presence of the zeolites in the composites. However, it is reasonable that the amplitude of the curves, which is the magnetization, is dependent on the mass of the non-magnetic zeolite. The curves coincide just above ~300 K, indicating that the blocking temperature of possible superparamagnetic particles is close/above to the room temperature.

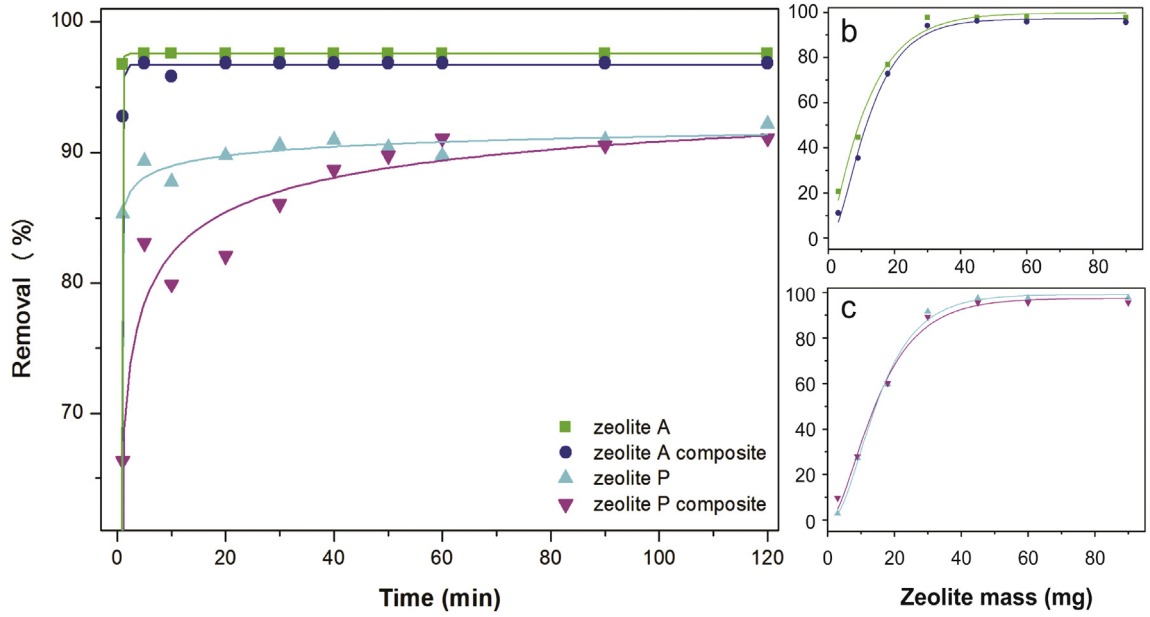

Fig. 9. Softening essays: (a) effect of contact time for 20 mL of 110 mg L^{-1} of Ca^{2+} solution with 30 mg of zeolites or 40 mg of the magnetic zeolite composites, (b) effect of zeolites mass and (c) effect of magnetic zeolite composites.

Thus, the observed ZFC and FC curves generally suggest large particle size, corroborating the results previously discussed, and nanoparticle anisotropy [63].

3.6. Water softening

The effect of contact time between the Ca^{2+} solution and the different materials used in this work over their efficiency as softeners is shown in Fig. 9(a). It is observed that after 5 min, zeolite A and its composite reduced the Ca^{2+} concentration in *ca.* 97%. Zeolite P reduced the Ca^{2+} concentration in almost 90%, also in few minutes, while the zeolite P magnetic composite showed similar efficiency. However, for the later to achieve this value, about 60 min was necessary. The relatively lower Si:Al ratio in zeolite P as well as a structure with a more limited accessibility for ions in solution accounts for a smaller efficiency in retaining Ca^{2+} compared to zeolite A, once it is expected lower amount of sites for exchangeable cations.

Fig. 9(b–c) shows the relation between the amount of used zeolite and the removal of Ca^{2+} for a given solution volume after 80 min of contact. There is no appreciable difference in the efficiency of the pure zeolite and the composites. The maximum adsorptive capacities found to each of the materials did not show great differences between the pairs, since zeolite A achieved the maximum of 74 mg g^{-1} and zeolite P, 75 mg g^{-1}; the zeolite A and P composites presented lower values of 54 and 51 mg g^{-1}, respectively, due the magnetite nanoparticles addition in the samples which do not exhibit pronounced adsorptive behavior.

4. Conclusions

In summary, in this paper we have performed a systematic study of the structural, spectroscopic and magnetic properties of zeolites A and P synthesized using kaolin as the main SiO_2 and Al_2O_3 sources by hydrothermal route, and of zeolite composites with magnetite nanoparticles.

In particular, kaolin has proved to be effective in the synthesis of zeolites A and P, the later by adding of supplementary silica. Magnetic composites based on zeolites A and P have been successfully obtained by aggregating magnetite nanoparticles over the zeolite surface in aqueous suspension. Neither the zeolite structures nor the magnetic properties of the nanoparticles have been affected when put together in the form of composites.

Thus, the results have evidenced that high quality zeolite composites with magnetite nanoparticles can be reached by considering the employed low cost method, placing this route as an attractive alternative for water softening, reaching high removal percentage for the zeolites and composites proposed.

Acknowledgments

The authors acknowledge the Laboratório Nacional de Nanotecnologia (LNNano/CNPEM) for experimental and technical support for the experiments of transmission electron microscopy, Central Analítica of Universidade Federal do Ceará (UFC/CT-INFRA/MCTI-SISNANO/Pró-Equipamentos CAPES) for the technical support and experiments of scanning electron microscopy, CNPq (process 402561/2007-4) and CAPES for financial support.

Appendix A. Supplementary data

Supplementary data related to this article can be found at http://dx.doi.org/10.1016/j.micromeso.2017.03.004

References

[1] A. Corma, Chem. Rev. 97 (1997) 2373–2419.
[2] C.S. Cundy, P.A. Cox, Microporous Mesoporous Mater. 82 (2005) 1–78.
[3] M. Moliner, F. Rey, A. Corma, Angew. Chem. Int. Ed. 52 (2013) 13880–13889.
[4] J. Cejka, R.E. Morris, D.P. Serrano, Catal. Sci. Technol. 6 (2016) 2465–2466.
[5] J. Weitkamp, Solid State Ion. 131 (2000) 175.
[6] K. Shams, S.J. Mirmohammadi, Microporous Mesoporous Mater. 106 (2007) 268–277.
[7] S. Chandrasekhar, P.N. Pramada, J. Porous Mater. 6 (1999) 283–297.
[8] D.W. Breck, Zeolites: Molecular Sieves, 1st ed., John Wiley & Sons, Inc., New York, 1974.
[9] J.C. Vartuli, G.J. Kennedy, B.A. Yoon, A. Malek, Microporous Mesoporous Mater. 38 (2000) 247–254.
[10] K. Abdmeziem, B. Siffert, Appl. Clay Sci. 8 (1994) 437–447.
[11] J. Aguado, D.P. Serrano, J.M. Escola, J.M. Rodríguez, Microporous Mesoporous Mater. 75 (2004) 41–49.
[12] C. Bebon, D. Colson, B. Marrot, J.P. Klein, F.D. Renzo, Microporous Mesoporous Mater. 53 (2002) 13–20.
[13] D. Boukadir, N. Bettahar, Z. Derriche, Ann. Chim. Sci. Mater. 227 (2002) 1–13.
[14] Y. Hu, X. Liu, Min. Eng. 16 (2003) 1279–1284.
[15] C. Busco, A. Barbaglia, M. Broyer, V. Bolis, G.M. Foddanu, P. Ugliengo, Thermochim. Acta 418 (2004) 3.
[16] L. Martins, D. Cardoso, Quim. Nova 29 (2006) 358–364.
[17] S.S. Jewur, Quim. Nova (1985) 99–105.
[18] D.-C. Lin, X.-W. Xu, F. Zuo, Y.-C. Long, Microporous Mesoporous Mater. 70 (2004) 63–70.
[19] D.M. Ruthven, Chem. Eng. Prog. Febr. (1988) 41.
[20] D. Akolekar, A. Chaffee, R.F. Howe, Zeolites 19 (1997) 359–365.
[21] R.T. Rigo, S.B.C. Pergher, D.I. Petkowicz, J.H.Z. dos Santos, Quim. Nova 32 (2009) 21–25.
[22] L. Ayele, J. Perez-Pariente, Y. Chebude, I. Diaz, Microporous Mesoporous Mater. 215 (2015) 29–36.
[23] Y.N. Ma, C.J. Yan, A. Alshameri, X.M. Qiu, C.Y. Zhou, D. Li, Adv. Powder Technol. 25 (2014) 495–499.
[24] J.Q. Wang, Y.X. Huang, Y.M. Pan, J.X. Mi, Microporous Mesoporous Mater. 199 (2014) 50–56.
[25] E.A. Hildebrando, C.G.B. Andrade, C.A.F. Rocha Junior, R.S. Angélica, F.R. Valenzuela-Diaz, R.F. Neves, Mater. Res. 17 (2014) 174–179.
[26] M.M. Acorsi, A.J. Schwanke, F.G. Penha, S.B.C. Pergher, D.I. Petkowicz, Cerâm. Ind. 14 (2009) 28–33.
[27] S.H. Silva Filho, L. Bieseki, A.R. Silva, A.A.B. Maia, R.A.S. San Gil, S.B.C. Pergher, Cerâmica 61 (2015) 409–413.
[28] E.B.G. Johnson, S.E. Arshad, Appl. Clay Sci. 97–98 (2014) 215–221.
[29] L.C.A. Oliveira, D.I. Petkowicz, A. Smaniotto, S.B.C. Pergher, Water Res. 38 (2004) 3699–3704.
[30] H. Aono, K. Tamura, E. Johan, T. Yamamoto, N. Matsue, T. Henmi, J. Am. Ceram. Soc. 96 (2013) 3218–3222.
[31] G. Nabiyouni, A. Shabani, S. Karimzadeh, J. Ghasemi, H. Ramazani, J. Mater, Sci. Mater. El. 26 (2015) 5677–5685.
[32] K. Barquist, S.C. Larsen, Microporous Mesoporous Mater. 130 (2010) 197–202.
[33] C. Belviso, E. Agostinelli, S. Belviso, F. Cavalcante, S. Pascucci, D. Peddis, G. Varvaro, S. Fiore, Microporous Mesoporous Mater. 202 (2015) 208–216.
[34] A.R. Loiola, J. Andrade, J.M. Sasaki, L.R.D. da Silva, J. Colloid Interface Science 367 (2012) 34–39.
[35] M. Yamaura, D.A. Fungaro, J. Mater. Sci. 48 (2013) 5093–5101.
[36] K. El-Sayed, Z.K. Heiba, A.M. Abdel-Rahman, Cryst. Res. Technol. 25 (1990) 305–312.
[37] L.S. Dubrovinskii, Y.Z. Nozik, Dokl. Akad. Nauk. SSSR 306 (1989) 1384–1386.
[38] M. Mehmel, Z. Kristallogr. Cryst. Mater. 90 (1935) 35.
[39] T. Ikeda, F. Izumi, T. Kodaira, T. Kamiyama, Chem. Mater. 10 (1998) 3996–4004.
[40] C. Baerlocher, W.M. Meier, Z. Kristallogr. Krist. Krist. Krist. 135 (1972) 339–354.
[41] L. Broussard, D.P. Shoemaker, J. Am, Chem. Soc. 82 (1960) 1041–1051.
[42] A.N. Fitch, H. Jobic, A. Renouprez, J. Phys. Chem. 90 (1986) 1311–1318.
[43] W.C. Hamilton, Phys. Rev. 110 (1958) 1050–1057.
[44] J.L. Hazemann, J.F. Berar, A. Manceau, Mater. Sci. Forum 79 (1991) 821–826.
[45] A.C. Larson, R.B. Von Dreele, Los Alamos National Laboratory Report LAUR, 2004, p. 86.
[46] B.H. Toby, J. Appl. Crystallogr. 34 (2001) 210–213.
[47] B.B. Kenne Diffo, A. Elimbi, M. Cyr, J. Dika Manga, H. Tchakoute Kouamo, J. Asian Ceram. Soc. 3 (2015) 130–138.
[48] A. Souri, F. Golestani-Fard, R. Naghizadeh, S. Veiseh, Appl. Clay Sci. 103 (2015) 34–39.
[49] C.I. Round, S.J. Hill, K. Latham, C.D. Williams, Microporous Mater. 11 (1997) 213–225.
[50] J.-Q. Wang, Y.-X. Huang, Y. Pan, J.-X. Mi, Microporous Mesoporous Mater. 199 (2014) 50–56.
[51] M. Gotic, S. Music, J. Mol. Struct. 834 (2007) 445–453.
[52] M. Kokate, K. Garadkar, A. Gole, J. Mater. Chem. A 1 (2013) 2022–2029.
[53] J.-l. Cao, X.-W. Liu, R. Fu, Z.-y. Tan, Sep. Purif. Technol. 63 (2008) 92–100.
[54] L.V.C. Rees, S. Chandrasekhar, Zeolites 13 (1993) 534–541.

[55] Y.V. Kolen'ko, M. Banobre-Lopez, C. Rodriguez-Abreu, E. Carbo-Argibay, A. Sailsman, Y. Pineiro-Redondo, M. Fatima Cerqueira, D.Y. Petrovykh, K. Kovnir, O.I. Lebedev, J. Rivas, J. Phys. Chem. C 118 (2014) 8691–8701.
[56] B.P. Jia, L. Gao, J. Am. Ceram. Soc. 89 (2006) 1739–1741.
[57] T. Iwasaki, N. Sato, K. Kosaka, S. Watano, T. Yanagida, T. Kawai, J. Alloys Compd. 509 (2011) L34–L37.
[58] H.L. Fan, B.Z. Song, Q.X. Li, Mater. Chem. Phys. 98 (2006) 148–153.
[59] M.S. Rahman, M. Whalen, G.A. Gagnon, Chem. Eng. J. (Lausanne) 234 (2013) 149–157.
[60] L.F. Cotica, V.F. Freitas, G.S. Dias, I.A. Santos, S.C. Vendrame, N.M. Khalil, R.M. Mainardes, M. Staruch, M. Jain, J. Magn, Magn. Mater. 324 (2012) 559–563.
[61] L.F. Cotica, I.A. Santos, E.M. Girotto, E.V. Ferri, A.A. Coelho, J. Appl. Phys. 108 (2010) 064325.
[62] B.D. Cullity, Introduction to Magnetic Materials, Addison-Wesley, Reading, 1972.
[63] R.A. Silva, M.J.L. Santos, A.W. Rinaldi, A.J.G. Zarbin, M.M. Oliveira, I.A. Santos, L.F. Cótica, A.A. Coellho, A.F. Rubira, E.M. Girotto, J. Solid State Chem. 180 (2007) 3545–3550.
[64] R.B. Gupta, Nanoparticle Technology for Drug Delivery, Taylor & Francis Group, New York, 2006.
[65] Z. Huang, F. Tang, J. Colloid Interface Sci. 275 (2004) 142–147.